Since January 2020 Elsevier has created a COVID-19 resource centre with free information in English and Mandarin on the novel coronavirus COVID-19. The COVID-19 resource centre is hosted on Elsevier Connect, the company's public news and information website.

Biosensors and Bioelectronics 176 (2021) 112942

Contents lists available at ScienceDirect

Biosensors and Bioelectronics

journal homepage: http://www.elsevier.com/locate/bios

Entropy-driven electrochemiluminescence ultra-sensitive detection strategy of NF-κB p50 as the regulator of cytokine storm

Kai Zhang [a,1], Zhenqiang Fan [a,1], Bo Yao [a,b], Tingting Zhang [c], Yuedi Ding [a], Sha Zhu [d], Minhao Xie [a,e,*]

[a] NHC Key Laboratory of Nuclear Medicine, Jiangsu Key Laboratory of Molecular Nuclear Medicine, Jiangsu Institute of Nuclear Medicine, Wuxi, Jiangsu, 214063, China
[b] Key Laboratory of Flexible Electronics (KLOFE) & Institute of Advanced Materials (IAM), Jiangsu National Synergetic Innovation Center for Advanced Materials (SICAM), Nanjing Tech University (NanjingTech), 30 South Puzhu Road, Nanjing, 211816, PR China
[c] Jiangsu Key Laboratory for Chemistry of Low-Dimensional Materials, School of Chemistry and Chemical Engineering, Huaiyin Normal University, Huaian, 223300, PR China
[d] Department of Oncology, The Affiliated Wuxi No.2 People's Hospital of Nanjing Medical University, Wuxi, 214000, PR China
[e] Department of Radiopharmaceuticals, School of Pharmacy, Nanjing Medical University, Nanjing, 211166, China

ARTICLE INFO

Keywords:
2019-nCoV
Transcription factors
GOAu−Ru composites
Entropy-driven
Electrochemiluminescence

ABSTRACT

2019 novel coronavirus (2019-nCoV) with strong contagion in the crowd, has ravaged worldwide and severely impacts the human health and epidemic prevention system, by producing a series of significant stress reactions in the body to induce further cytokine storm. Transcription factors (TFs) served as essential DNA binding proteins play an integral role in regulating cytokine storm, and the detection of it in the human coronavirus environment provides especially valuable approaches to diagnosis and treatment of 2019-nCoV and development of antiviral drugs. In this work, an entropy-driven electrochemiluminescence (ECL) biosensor was constructed for ultra-sensitive bioassay of NF-κB p50. The strategy primarily capitalizing the splendid double-stranded DNA (dsDNA) binding properties of transcription factors, employing GOAu-Ru composite material as ECL emitter, utilizing entropy-driven reactions for signal amplification method, offered a repeatable proposal for TFs detection. In the absence of TFs, the released DNA1 further went in the entropy-driven reaction, contributing to an "ECL off" state. However, in the presence of TFs, the dsDNA avoided being digested, which blocked DNA1 for participating in the entropy-driven reaction, and the system exhibited an "ECL on" state. Most importantly, the ECL bioanalytical method denoted broad application prospects for NF-κB p50 detection with a lower detection limit (9.1 pM).

1. Introduction

Since the emergence of the 2019 novel coronavirus (2019-nCoV) in December 2019, the epidemic of the novel coronavirus disease (COVID-19) has rapidly emerged and wildly spread across the world. In addition to the respiratory symptoms in the majority of SARS-COV-2 treatments, some patients also show gastrointestinal symptoms or even appear asymptomatic. According to related studies, the 2019-nCoV may cause damage to other organs than the lungs, such as the heart, kidneys and pancreas (Huang et al., 2020). Individual patients may also experience central nervous system symptoms, for instance, including convulsions, dizziness, knee hyperreflexia, and limb tension (Guan et al., 2020). Laboratory tests have shown that the blood physicochemical environment of the severe patients changed significantly. For example, lymphocytes and blood oxygen saturation decreased obviously, accompanied by an increase of lactate dehydrogenase (LDH) and C-reactive protein as well as triggering a cytokine storm caused by the surge of various pro-inflammatory cytokines (Terpos et al., 2020). Transcription factors (TFs) as significant pathological indicators are DNA binding proteins that bind to related sequences of gene promoter or enhancer to regulate gene expression, acting a pivotal role in the research of human coronavirus and treatment of 2019-nCoV by

* Corresponding author. NHC Key Laboratory of Nuclear Medicine, Jiangsu Key Laboratory of Molecular Nuclear Medicine, Jiangsu Institute of Nuclear Medicine, Wuxi, Jiangsu, 214063, China.
E-mail address: xieminhao@jsinm.org (M. Xie).
[1] These authors contributed equally to this work.

https://doi.org/10.1016/j.bios.2020.112942
Received 11 September 2020; Received in revised form 19 December 2020; Accepted 24 December 2020
Available online 30 December 2020

regulating cytokine storm expression (Mahmudpour et al., 2020; Markopoulos et al., 2019). Nuclear factor kappa-light-chain-enhancer of activated B cells (NF-κB) p50 as a crucial pleiotropic transcription factor, has shown significant value in fundamental researches related to cell differentiation, apoptosis, inflammation and tumorigenesis (Potoyan et al., 2016). The quantitative detection of NF-κB p50 is of paramount and far-reaching significance for precisely diagnosing inflammation, comprehensively assessing viral damage to human, and developing antiviral drugs under the circumstances that COVID-19 continue to rage.

Traditional methods for detecting transcription factors include electrophoretic mobility shift assay (EMSA), DNA footprinting, western blot, and enzyme-linked immunosorbent assay (ELISA), etc.(Cao and Zhang 2013; Zhang et al., 2012). Among them, EMSA, DNA footprinting, and western blot can only perform qualitative or semi-quantitative analysis on transcription factors, and are incapable of meeting contemporary requirements for fast, environmentally friendly and accurate detection. For example, EMSA, as the golden-standard method for studying the vitro binding property of TFs, facing the problems of using radioisotope and unstable probe, which can cause potential radiation damage to the human body and high autoradiographic background (Zhang et al., 2020). Although biotin-labeled chemiluminescent probes have been widely used, the extension of this type of method is problematic because it is not suitable for precise quantification, and the experiments are time-consuming (up to 48 h) and generate only a few TFs binding data (Hlavac and VandeVord 2019). DNA footprinting is commonly used to determine the binding sequence of transcription factors, but it also comes with a radioisotopes problem (Parks et al., 1996). Antibody labeling is needed in western blot, increasing the cost of material expenditure during the experiment (Jiang et al., 2009). ELISA can achieve high-throughput quantitative detection of transcription factors with relatively high sensitivity already down to nanomolar (nM) concentration limits of detection (LOD) using double-stranded DNA binding ability, but expensive nuclear chromatin immunoprecipitation-level primary antibodies are often required, bringing out higher cost (Gao et al., 2020; Shao et al., 2005). Besides, the experiments are prone to be interfered by the reacted temperature and time, which causes false-positive results for the tests (Holzhauser et al., 2002).

In recent years, the detection strategies for transcription factors mainly include the fluorescence method, electrochemical method, and colorimetric method. Among all these methods, electrochemiluminescence (ECL) produced by the electric field generated between the electrodes to excite the emitters to cause electronic excitation, transition, and light emitting, which combines the merits of spectroscopy and electrochemistry, has attracted widespread attention and shown enormous application value in bioanalysis (Nie et al., 2019; Xu et al., 2019; Ye et al., 2019; Zhang et al., 2019a). ECL method not only overcomes the shortcomings of high background and excitation light interference of fluorescence analysis and electrochemical signals that are affected by current disturbances caused by temperature and humidity changes, but also has the characteristics of high sensitivity and simple equipment as electrochemical analysis, and the excellent selectivity as fluorescence method owing to the unique spectral characteristics of each emitter molecule (Ge et al., 2019; Lin et al., 2019; Yin et al., 2014). In addition, ECL analysis also avoids the problem that some chemiluminescent reagents are laborious to deposit or unstable to use under specific circumstance. For example, gold nanoparticles participated colorimetric reaction, exists a situation where gold nanoparticles tend to aggregate which makes it difficult to reuse and extremely reduces the reproducibility of the assays (Chen et al., 2014). In various ECL biosensing systems, tris (2,2′-bipyridyl)-ruthenium (II) ($Ru(bpy)_3^{2+}$) and its derivatives were commonly used for ECL emitters (Zhang et al., 2017). For the fact that the $Ru(bpy)_3^{2+}$ ECL system consumes more emitting materials in the homogeneous solution, therefore, the stability of the system is affected, which greatly cuts down the detection efficiency and highly increases the cost.

With the advance of nanotechnology, researchers are devoted to the combination of ECL emitters and nanotechnology, and the traditional Ru $(bpy)_3^{2+}$ emitter with splendid ECL efficiency ushered in a new vitality for electrochemiluminescence biosensing. (Nie et al., 2019; Ye et al., 2019). Generally, $Ru(bpy)_3^{2+}$ derivatives existing in nanomaterials are mainly divided into two categories. One category is the $Ru(bpy)_3^{2+}$ derivatives as adsorption molecules, doped into the nanomaterials through electrostatic adsorption, coordination interaction, cross-linking and physical doping, etc., the primary carriers of which, for instance, are liposomes, silica, quantum dots, precious metal nanomaterials, and 3D metal-organic frameworks (MOF)(Jiang et al., 2019; Yang et al., 2018). The composites of $Ru(bpy)_3^{2+}$ derivatives and other carrier nanomaterials are then used as ECL emitters for the fabrication of ECL biosensors and provide a fundamental basis in bioanalysis and clinical diagnosis. Although the loading procedure causes it cumbersome for the material modification, the emitters' loading strategies provide huge surface area for the emitters to attach and significantly improve the emitting intensity of luminescent molecules. The other category is that $Ru(bpy)_3^{2+}$ derivatives are served as the important components of the precursors for the synthesis of nanomaterials with various morphologies. For example, Chen et al. made polyethyleneimine-ruthenium (PEI-Ru) complex a precursor to prepare hollow porous polymer nanospheres (Ru-HPNSs), which further served as ECL emitter for the fabrication of ultra-sensitive aptamer sensor of mucin 1 assay (Chen et al., 2017). Collinson et al. putting ECL precursors, ruthenium-tripropylamine (TPA) trapped in a porous silicate host matrix to construct solid structure under room condition, realizing the staple light emission at ultramicroelectrodes (Collinson et al., 1999). In general, by integrating with nanotechnology, the loading amount of Ru $(bpy)_3^{2+}$ derivatives and stability of the biosensing systems were obviously heightened, which effectively lessened the leakage of ECL emitters in aqueous. Therefore, the application of nanotechnology to the preparation of ECL emitter nanocomposites is enormously significant for improving the ECL efficiency and enhancing the ECL-based biosensing platforms.

DNA nanomachines refer to a class of biomolecular components similar to functional machines. In 1982, Seeman pioneered the research field of DNA nanomachine technology for the first time (Seeman 1982). In 2006, Rothemund's team constructed DNA origami technology and assembled "smiley face", "five-pointed" star and other shapes (Rothemund 2006). Zhou et al. created a new type of light-responsive nanomachine, the target DNA substrate chain with two "arm" structures. This newly constructed nanomachine can also be used in vivo to regulate gene expression through antisense strategies, or used in vitro to switch the mechanical movement of nanorobots. Because of the high specificity of the ribozyme (DNAzyme) and no need for additional protease for cleavage, it can be widely used in nucleic acid-sensing (Zhou et al., 2010). We also proposed a unique and formidable DNA nanomachine, which combines tandem strand displacement reaction with DNA molecular machines, realizing the detection of ion channels on the cell membrane (Zhang et al., 2019b). As the entropy-driven reaction happened on the gold electrode, numerous ferrocene (Fc) labeled DNA was modified on the Au electrode surface, resulting in a changed electrochemical signal.

DNA nanomachines also have many significant advantages. DNA oligonucleotides, as its constituent components obtained by chemical method, are capable of being modified with easily technological approaches, which makes it easy for DNA nanomachines to construct and characterize. Besides, DNA sequences can design freely. The assembly of a variety of DNA nanostructures based on specific base pairing can achieve successfully, to make it easy for nanomachines to design according to the detection needs. Therefore, DNA nanomachines can widely use in biomolecules and tumor cells detection, cell imaging, and cancer treatment. Researchers have already constructed many DNA nanomachines with various structures and functions, such as DNA walker, DNA tweezer, DNA motor DNA gear and so on (Bath et al., 2005;

Brutzer et al., 2012; Chen et al., 2019; Huang et al., 2019; Li et al., 2010).

Based on the above research background, an ultra-sensitive biosensor for NF-κB p50 detection system, on the basis of entropy-driven reaction and $Ru(bpy)_3^{2+}$ modified graphene oxide (GO) ECL emitter is proposed. The strategy we designed can achieve ultra-sensitive detection of the target to be tested without the aid of nicking enzymes (Exo III). Therefore, this method does not require a strict temperature control process to weaken the interference of environmental conditions and ensure the stability of the testing. For that the modification process and the entropy-driven reaction are barely occurred on the electrode; only a simple operation is required in our assays. This work not only realized the ultra-sensitive detection of NF-κB p50, but also provided valuable ideas for solving the problems related to transcription factors caused by the novel coronavirus cytokine storm.

2. Materials and method

2.1. Reagents and chemicals

The oligonucleotides purified by high-performance liquid chromatography (HPLC) used in our detection strategy were obtained from Genscript Biotech. Co., Ltd. (Nanjing, China) with the sequences, as shown in Table S1. Silver nitrate ($AgNO_3$) and sodium borohydride ($NaBH_4$) were bought from Boer Chemical Reagent Co. Ltd. (Shanghai, China) and Sinopharm Chemical Reagent Co. Ltd. (Shanghai, China), respectively. The gel and buffer for non-denaturing polyacrylamide gel electrophoresis (PAGE) and exonuclease III (Exo III) for the cleave process were obtained from Sangon Biotech Co. Ltd. (Shanghai). NF-κB p50 (human recombinant) and dehydroxymethylepoxyquinomicin ((−)-DHMEQ) were got from Hengfei Biotechnology Co. Ltd. (Shanghai) and MedChemExpress (New Jersey, U.S.A), respectively. 1-ethyl-3-(3-dimethyllaminopropyl)-carbodiimide hydrochloride (EDC) and N-hydroxysuccinimide (NHS) were both from Aladdin Reagent (Shanghai, China). Tris (4,4′-dicarboxylic acid-2,2′-bipyridyl) ruthenium (II) dicbloride ($Ru(dcbpy)_3^{2+}$) and polyethylenimine (PEI) modified graphene oxide nanosheets (GO-PEI) were obtained from XFNANO (Nanjing, China). In addition, other analytical grade general chemicals and reagents used to prepare the buffers in this research, unless otherwise stated, were acquired from Aladdin Reagent (Shanghai, China), and the ultrapure water was processed through Milli-Q purification system.

2.2. Instruments and measurements

Transmission electron microscopy (TEM) measurements were obtained from 1400 PLUS (Japanese electronics). X-ray Photoelectron Spectroscopy (XPS) and fourier transform infrared spectroscopy (FT-IR) spectra ranged from 4000−500 cm^{-1} were got from Thermo Fisher K-Alpha and Thermo Fisher Nicolet iS5, respectively. ECL experiments were collected by ECL-6B instrument built by State Key Laboratory of Analytical Chemistry for Life Science, Nanjing University. The voltage was scanned from 0 to 1.3 V, with the medium scan rate (0.1 V/s). The three-electrode system which contained a glassy carbon electrode (GCE) 3 mm in diameter, an Ag/AgCl reference electrode, a platinum counter electrode were used. UV–vis absorption spectra were got from Spectra Max M5e (Molecular Devices Co. Ltd). The electrolyte used in the ECL quantitative assays was phosphate buffer saline (PBS) (0.1 M, pH 7.4). Both cyclic voltammetry (CV) and impedance spectra were obtained in PBS buffer (0.1 M, pH = 7.4) containing $[Fe(CN)_6]^{3-/4-}$ (5 mM). The scan rate for CV spectra was 100 mV/s, and the frequency for the impedance plot was from 100 kHz to 0.1 Hz.

2.3. Synthesis of GOAu-Ru

The synthesis of GOAu-Ru was referring to the work of Ye et al. with slight modifications (Ye et al., 2019). Firstly, $Ru(dcbpy)_3^{2+}$ aqueous solution (5 mL, 2 mg mL^{-1}) was pre-prepared. After that, 5 mL mixture of EDC (2 mg mL^{-1}) and NHS (1 mg mL^{-1}) was added to the $Ru(dcbpy)_3^{2+}$ aqueous solution with stirring for 2 h to activate the –COOH of $Ru(dcbpy)_3^{2+}$. Then 10 mL GO-PEI solution (1 mg mL^{-1}) was injected into the above activation solution under magnetic stirring and continued to react for 2 h. Next, 10 mL 13-nm-sized Au nanoparticles were added to the prepared GOAu-Ru hybrid with continuous stirring for 2 h to form electrostatic interaction based on Au–N bond. For removing redundant reagents, serval centrifugations were performed. Finally, GOAu-Ru was diluted into 4 mL purified water for further use.

2.4. Preparation of AgNC

The preparation of Ag nanocluster (AgNC) was referring our previous work with few modifications, which was briefly illustrated as followed (Fan et al., 2019). Initially, $AgNO_3$ solution (10 μL, 25 mM) was mixed with DNA6 solution (1 mL, 30 μM, 5.0 mM Mg^{2+} in 0.1 M PBS solution, pH 7.4), in which the molar ratio of Ag^+ to template DNA was around 8:1. The mixture was then intensely shocked (2 min), followed by adding $NaBH_4$ solution (15 μL, 25 mM) just as-prepared at 0 °C condition. Continue to oscillate for 1.5 h violently, and the reaction solution was put into the refrigerator (4 °C) for 12 h to synthesize AgNC.

2.5. Fabrication of ECL biosensor

Firstly, the DNA hybrid PBS solution was prepared as followed. Initially, DNA3, DNA4 and DNA5 with the same final concentration (1 μM) were put into PBS buffer (pH 7.4), which contained $MgCl_2$ (5.0 mM) and TCEP (0.1 mM) and incubated at 25 °C for 1.5 h to cut off the disulfide bond. Next, the DNA mixture solution was heated up in the range of 90–95 °C for breaking hydrogen bonds within hybridized single-stranded DNA (ssDNA), quickly cooled to room temperature to constitute hybrid DNA probe and stored at 4 °C for further use.

Secondly, the GCE (4 mm diameter) was continuously grinded by 0.05-μm-sized alumina, alternately sonicated in deionized water for getting a spotless mirror. Then 8 μL of GOAu-Ru suspension was put onto the already cleaned GCE (abbreviation as GOAu–Ru/GCE) and dried at a nitrogen atmosphere. After that, the GOAu-Ru/GCE was dipped into a DNA hybrid PBS buffer solution overnight to connect the hybrid DNA probe (abbreviation as hybrid DNA/GOAu-Ru/GCE) through the formation of Au–S bond.

Thirdly, the hybrid DNA/GOAu-Ru/GCE was dipped into 60 μL PBS solution (0.1 M, pH 7.4), which contained 100 μM 6-mercaptohexanol (MCH) for passivating the unoccupied sites outsides specific hybrid DNA probe of the modified GCE and facilitate the hybrid DNA probe oriented vertically to the GCE surface. In addition, after each modification, the GCE needed to be rinsed with PBS solution (20 mM) for removing substances that were not specifically adsorbed. Thus, the construct of ECL biosensor (MCH/hybrid DNA/GOAu-Ru/GCE) was achieved.

2.6. Quantification assay

Initially, DNA duplexes (10 μM) were constituted by mixing DNA1 and DNA2 in DNA hybridization buffer containing Tris–HCl (50 mM, pH 8.0), NaCl (100 mM) and EDTA (1 mM). Next, the mixture solution was heated up to 90–95 °C and followed by cooling down to 4 °C immediately for the formation of double-stranded DNA (dsDNA) with high purity and highly structural rigidity. After that, the dsDNA (50 μL) solution mixed with a series of concentrations of NF-κB p50 (20 μL) in transcription factor binding solution which consisted of Tris–HCl (10 mM, pH 8.0), KCl (100 mM), $MgCl_2$ (2 mM), EDTA (0.1 mM), 10% glycerol, DTT (0.25 mM) and incubated for 45 min at 25 °C to construct a complex of dsDNA and NF-κB p50. In addition, in order to evaluate the effect of endogenous substances of cell nuclear extracts, various concentrations of NF-κB p50 in diluted nuclear extracts (20 μL) were also

incubated separately with 50 μL dsDNA solution in transcription factor binding solution for 45 min at 25 °C.

For the exonuclease III (Exo III) cleavage process, the protein binding solution after incubation was added 50 μL of Exo III (2 U μL^{-1}) to react for 15 min at 37 °C. And then, the mixture solution was slowly heated to 75 °C and held for 10 min to cease the cleavage process. Therefore, the reaction solution was prepared, which was ready for the next assay procedure. After that, the already fabricated ECL biosensor was dipped into 100 μL reaction solution and kept incubating at 25 °C for 40 min. Immediately afterwards, AgNC was added to the reaction solution and continued at 25 °C (1 h). Last but not least, the processed ECL biosensor was flushed by PBS solution (20 mM, pH 7.4) before ECL tests with PBS solution (0.1 M, pH 7.4) ranged from –1–1.3 V under the presence of co-reactant tripropylamine (10 mM).

2.7. Gel electrophoresis

Nondenaturing PAGE choose PAGE gel (12%) to characterize the DNA hybridization process, using Tris-borate-EDTA (TBE) running buffer (89 mM Tris, 89 mM boric acid and 2 mM EDTA, pH 8.0–8.5) under the voltage of 90 V for 2 h. DNA samples (20 μL) mixing with 1×loading buffer containing 0.25% bromophenol blue and 60% glycerol were pre-prepared and loaded into the well of the gel, respectively. After the running process, the gel was stained with ethidium bromide (EB) for 20 min under shaking and photographed by the gel image system (ChemiDoc MP, Bio-Rad).

2.8. Cell culture and treatment

The process of cell culture was briefly illustrated as followed. Firstly, HeLa cells were implemented in cell cultural medium (RPMI-1640) with the addition of 10% fetal bovine, 100 μg mL^{-1} penicillin, and streptomycin in moist air (containing 5% CO_2). Then the cultured cells were incubated with TNF-α (PeproTech) for 30 min. In the cell nuclear extraction experiments, the HeLa cells nuclear extracts were acquired by nucleoprotein extraction kit (Active Motif), and eventually diluted into 300 μL for further exploring the endogenous influences of other proteins in cell nuclear.

3. Results and discussion

3.1. The principle of entropy-driven reaction for NF-κB p50 detection

The new strategy of NF-κB p50 detection we designed mainly includes the exonuclease III (Exo III) assisted nicking enzyme reaction, and entropy-driven reaction participated ECL assays (Scheme 1). When NF-κB p50 is present in the system, the binding site on the double-stranded DNA (dsDNA, DNA1/DNA2 duplex) can bind to NF-κB p50, and the resulting composite structure can hinder the cleavage of the double-stranded DNA by exonuclease III. After treating the electrode with this reaction system, the reaction on the electrode surface cannot be triggered so that a high ECL signal can be detected. When there is no NF-κB p50 in the system, the Exo III can digest the 3′ blunt end and the concave

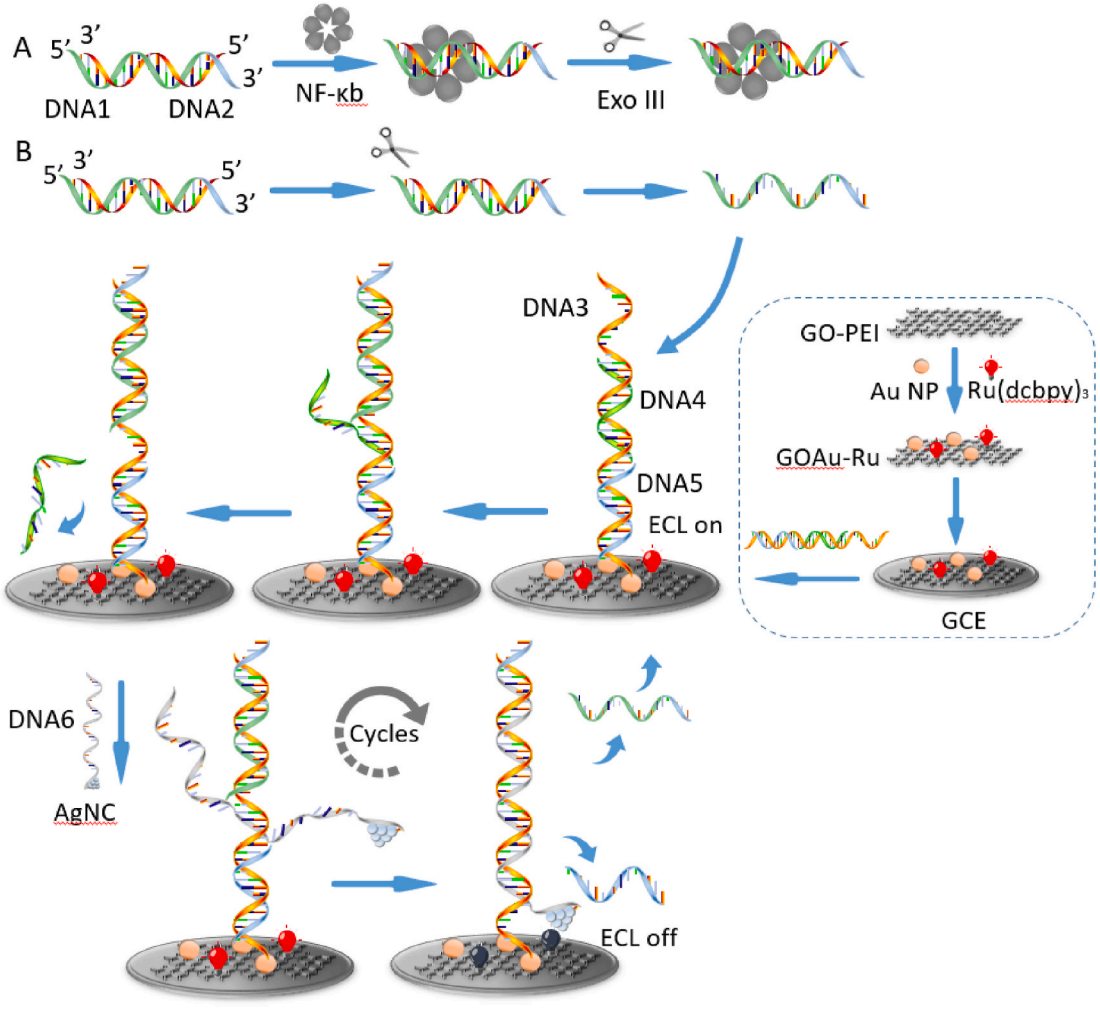

Scheme 1. Schematic diagram of entropy-driven electrochemiluminescence biosensor for ultra-sensitive detection of NF-κB p50.

end of the single-stranded DNA in the double-stranded DNA, so it can specifically cut the double-stranded DNA from the 3′ end to the 5′ end DNA2 in DNA1/2 duplex. In addition, because we specially designed DNA3 to have a five-base protrusion at the 3' end, it prevented DNA1 from being digested by exonuclease III. After the DNA2 is digested, the free DNA1 will undergo an entropy reduction reaction with the modified DNA3/4/5 complex on the electrode. First, DNA1 binds to the naked single-stranded portion of DNA3, and further hybridizes with DNA3 to form a double-stranded DNA1/3, which eventually causes DNA4 to be replaced. In the formed DNA3/1/5, there is a partial base sequence in the middle portion of DNA3, which can hybridize and pair with AgNC modified DNA6, and further form DNA3/6 double-stranded DNA. The replaced DNA1 can further trigger the rest of the entropy-driven DNA reaction. Since the silver nanoclusters modified at the end of DNA6 can quench the ECL signal on the electrode surface, the biosensor after the reaction obtained a low ECL signal.

3.2. Characterization of GOAu−Ru composites

The TEM image showed that the Au nanoparticles (AuNPs) were dispersed in the GO-Ru hybrid (Fig. 1A), and the dynamic light scattering (DLS) data (inset in Fig. 1A) indicated the size of the AuNPs was approximately 13 nm. UV–vis spectra were further employed to characterize the successful synthesis of the GOAu-Ru hybrid, as depicted in Fig. 1B. The absorbance peaks of $Ru(dcbpy)_3^{2+}$ were centered at 304 and 475 nm for the distinctly functional groups (carboxyl and bipyridyl rings), GO-PEI showed a characteristic peak at 239 nm on account of the existence of graphene oxide (GO) and Au NPs had obvious plasma absorption peak approximately at 519 nm, which were all in line with the corresponding absorbance peaks in GOAu-Ru hybrid. From the evidence that the absorption peaks of GOAu-Ru hybrid were consistent with that of other synthetic components, we could get a preliminary conclusion that GOAu-Ru hybrid was synthesized successfully. Furthermore, the formation of GOAu−Ru hybrid was confirmed by XPS spectra, as showed in Fig. 1C. Typically, the GOAu−Ru hybrid showed 284.8 eV, 399.8 eV, 531.1 and 482.1 eV for C1s, N1s, O1s and Ru3p. Additionally, the characteristic doublet of Au 4f was depicted in Fig. 1D. The Au 4f showed two characteristic peaks at 83.3 eV (Au 4 $f_{7/2}$) and 86.9 eV (Au 4 $f_{5/2}$), by which the spin-orbit splitting of the doublet calculated was 3.6 eV, indicating the presence of Au NPs. The Fourier transform infrared spectroscopy (FT-IR) supply more verification for the synthesis of GOAu-Ru (Fig. S1). The primary functional group in GO-PEI contained –OH demonstrated in 3430 cm^{-1}, with two noticeable peaks at 2903 and 2878 cm^{-1} which were separately in line with stretching vibration of $–CH_2$ and amide characteristic peak at 1616 cm^{-1}. Besides, the GOAu−Ru presented the same peaks which matched well with typical absorption bands of GO-PEI, the apparent increase peak at 1616 cm^{-1} without the peak at 1735 cm^{-1} assigned to C═O of the carboxyl, further indicating the carboxyl in the $Ru(dcbpy)_3^{2+}$ was totally changed into amide. The XPS and FT-IR characterizations both verified the formation of GOAu−Ru hybrid. Additionally, elemental mapping was utilized to illustrate the elemental distribution of the GOAu−Ru (Fig. 2). The main elements of $Ru(dcbpy)_3^{2+}$ containing ruthenium (Fig. 2C) and nitrogen (Fig. 2E) were evenly distributed on the surface of GO which was identified by carbon (Fig. 2D) and oxygen elements (Fig. 2G), and the Au (Fig. 2F) showed that Au NPs were successfully anchored on the GO-Ru hybrid.

3.3. Nondenaturing PAGE for the entropy-driven strategy

Afterwards, PAGE was used to verify the feasibility of the amplification strategy. As depicted in Fig. 3A, Lane 1 (DNA1), Lane 2 (DNA6) were served as control stripes and each showed a single stripe. The stripe of dsDNA probe hybridized by DNA3 and DNA6 was in Lane 4. The hybridization of DNA3, DNA4 and DNA5 (Lane 3) led a single bright band indicating the hybridization reaction was fully achieved. Afterwards, as the hybridized DNA probe was incubated with DNA6 (Lane 5), notably, a stripe at the same level as DNA3/6 was observed. At the same time, a vaguely fastest band appeared, which was speculated to be DNA5. Because DNA4 and DNA1 have the same number of bases, the two bands showed the same level on the PAGE image. The band above the DNA5 was therefore considered as DNA4. Previous work also confirmed this interesting phenomenon (Zhang et al., 2007). When the DNA1 was reacted with DNA3/4/5 complex (Lane 6), the bands' positions were consistent with that of the DNA3/1/5 and DNA4 as speculated. However, when DNA6 was added into the reaction of DNA3/4/5 with DNA1, brighter dsDNA stripe of DNA3/6 and DNA5 compared to that in Lane 5 were observed, indicating that the entropy-driven reaction could be extremely triggered by DNA1 and then exposed toehold for next hybridization of DNA6 to produce more DNA3/6 and expel more DNA5. Therefore, we could infer that the PAGE images visually demonstrated the feasibility of the entropy-driven reaction.

3.4. ECL mechanism of emitters

We first obtained the fluorescence spectrum (Fig. 3B, black curve) the and the ECL spectrum (Fig. 3B, red curve) through the spectrophotometer and optical filters, separately. The maximum ECL emission wavelength of GOAu-Ru was at 622 nm, and the fluorescence emission spectrum had a maximum value at 637 nm. Compared to the fluorescence spectrum of GOAu-Ru, the ECL spectrum assumes a hypsochromic shift, presumably the reason that GO and Au nanoparticles with high

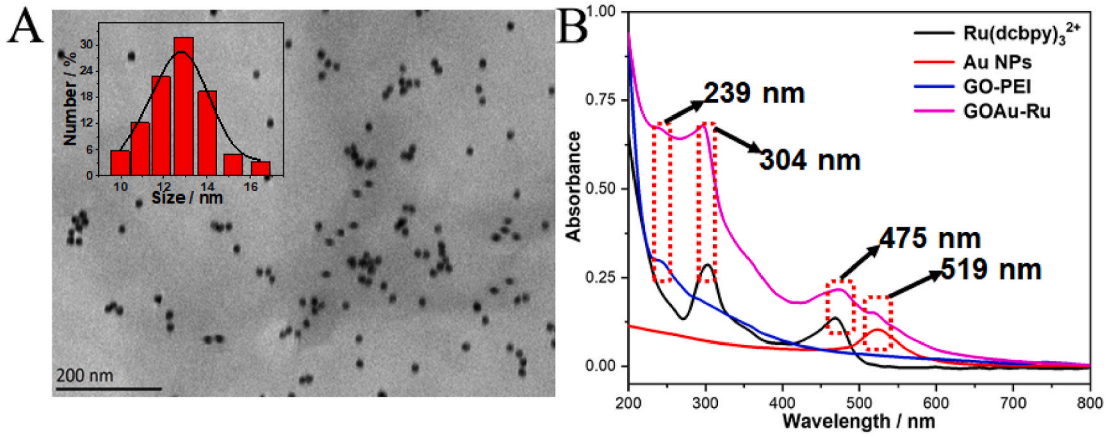

Fig. 1. (A) TEM characterization of GOAu−Ru and DLS of Au nanoparticles (inset of Fig. 1A). (B) UV–vis spectra of GOAu-Ru and its synthetic materials (Ru $(dcbpy)_3^{2+}$, Au NPs, and GO-PEI).

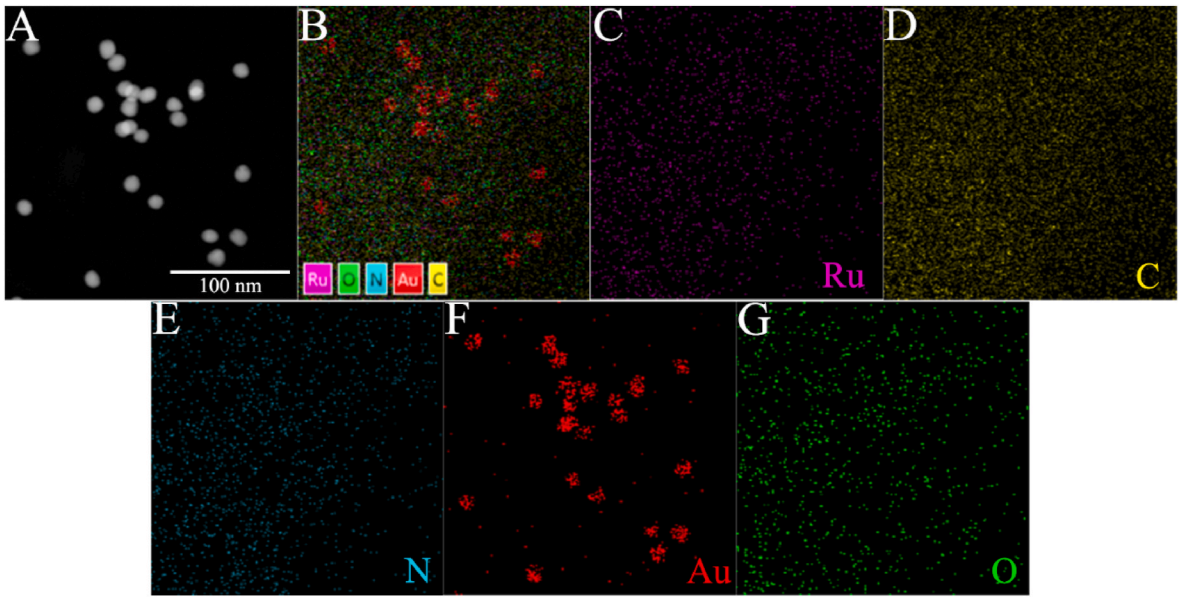

Fig. 2. Electron images of GOAu−Ru (A), EDS overlays (B), and elemental mapping of Ru (C), C (D), N (E), Au (F), and O (G).

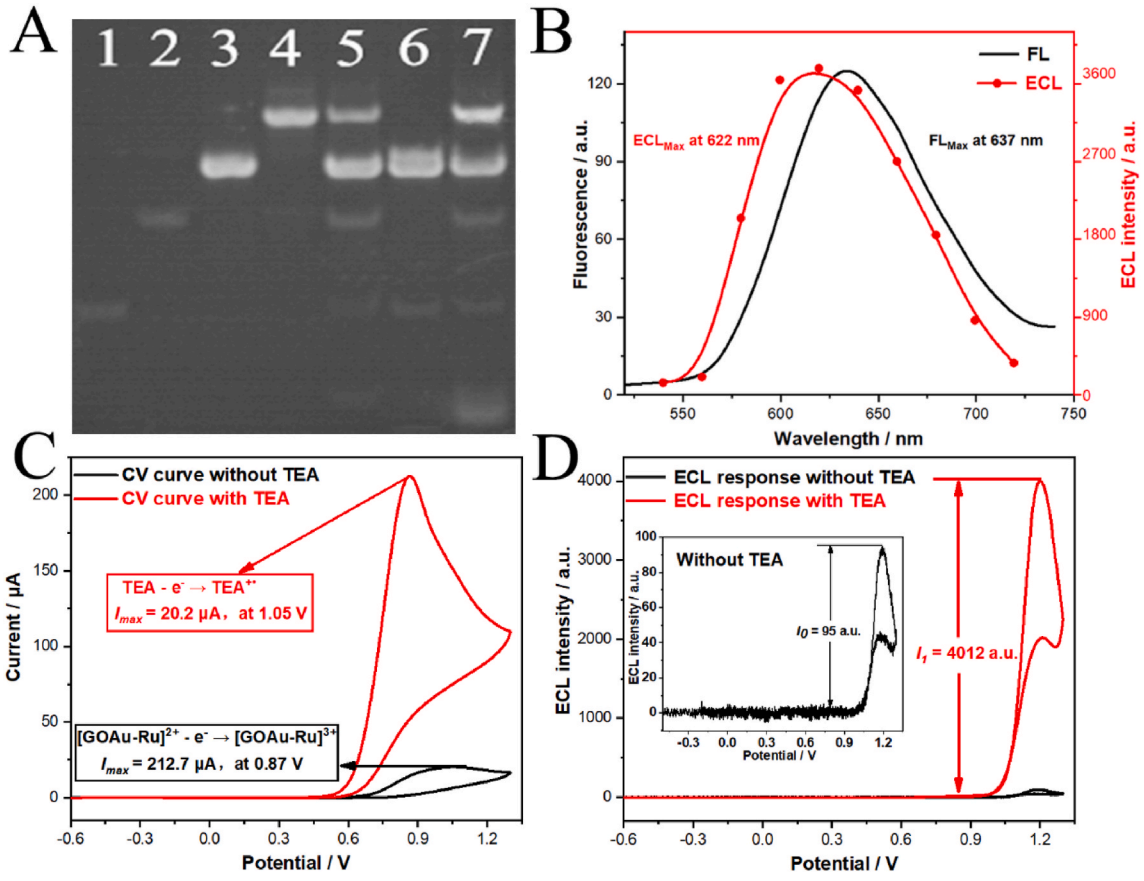

Fig. 3. (A) PAGE characterization of the entropy-driven reaction. Lane 1, 2 were DNA1 (1 μM) and DNA6 (1 μM); Lane 3, 4 were the hybridized DNA3/4/5 (1 μM) and DNA3/6 complex probe (1 μM); Lane 5 and Lane 6 showed that 1 μM hybridized DNA3/4/5 probe reacted with 1 μM DNA6 and 1 μM DNA1, respectively. Lane 7 revealed the entropy-reaction that 1 μM hybridized DNA3/4/5 probe incubated with DNA1, and then reacted with DNA6. (B) Fluorescence and ECL spectra of GOAu-Ru. (C) CV curves and (D) ECL-potential plots of GOAu-Ru in PBS buffer with or without 25 mM co-reactant TEA. The inset of (D) was the magnified image of the ECL curve without co-reactant.

electron transfer efficiency, increase the energy of transition. Next, for the clarification of the ECL mechanism of emitter composites, Fig. 3C and D listed the simultaneous CV and ECL signal responses in different assay conditions. The CV curve of GOAu-Ru exhibited a feeble signal response at 1.05 V, indicating that $[GOAu\text{-}Ru]^{3+}$ was generated by losing electrons. For the assay solution with co-reactant triethylamine

(TEA), the electrical oxidation of TEA was attributed to a significant oxidation peak at 0.87 V. When GOAu-Ru/GCE was detected in assay condition without TEA, feeble ECL signals were observed. Since TEA dissolved in the solution acted as co-reactant for the emitting process, the ECL intensity was much higher than that in the assay solution without co-reactant. The whole evidence showed that GOAu-Ru is served as ECL emitter, and TEA was acted as a co-reactant to improve ECL efficiency. According to the experimental phenomenon above and earlier work, the anode mechanism of GOAu-Ru with co-reactant TEA is illustrated below. Firstly, TEA and $[GOAu\text{-}Ru]^{2+}$ are electrochemically oxidized to $TEA^{+\bullet}$ and $[GOAu\text{-}Ru]^{3+}$ (Equations (1) and (2)). Then, $TEA^{+\bullet}$ loses hydrogen cation and converts to $TEA^{\bullet}$ with strong reducibility, which further reacts with $[GOAu\text{-}Ru]^{3+}$ to beget excited states $[GOAu\text{-}Ru]^{2+*}$ (Equation (3)). Lastly, the energy of unsteady excited state dissipates and produces optical light to return to the ground states (Equation (4)).

$$TEA - e^- \rightarrow TEA^{+\bullet} \rightarrow TEA^{\bullet} + H^+ \quad (1)$$

$$[GOAu\text{-}Ru]^{2+} - e^- \rightarrow [GOAu\text{-}Ru]^{3+} \quad (2)$$

$$[GOAu\text{-}Ru]^{3+} + TEA^{\bullet} \rightarrow [GOAu\text{-}Ru]^{2+*} + product \quad (3)$$

$$[GOAu\text{-}Ru]^{2+*} \rightarrow [GOAu\text{-}Ru]^{2+} + h\nu \quad (4)$$

3.5. Characterization during the stepwise modifications of the GCE

Firstly, CV was used to characterize the progressively modified GCE as shown in Fig. 4A. The GCE before modification presented a redox peak, while with the modification of GOAu-Ru, the CV signal peak gone down noticeably. After the hybrid DNA probes, MCH, DNA1 by degrees modified to the GOAu-Ru/GCE, the redox peaks successively declined, mainly due to the increased impedance of charge transfer. However, with the AgNC modified DNA6 immobilized to the electrode, the redox peak was obviously raised, for that the AgNC increased the efficiency of electron transfer. Next, electrochemical impedance spectroscopy (EIS) was further employed to describe the surface impedance after each stepwise modification. In Fig. 4B, as the classical model circuit illustrated, the total impedances composed of real Z' and imaginary Z'', were reflected by circuit elements in the form of circuit diagram, which mainly related to the resistance and capacitance of the electrochemical system. The real Z' chiefly included electrolyte's ohmic resistance (*Rs*), the impedance of charge transfer (*Rct*), and Warburg diffusion impedance (*W*). In this three-electrode system, *Rs* reflected the resistance between GCE and the Ag/AgCl reference electrode, *Rct* corresponded the interfacial impedance of electrode, which was incarnated by the semicircle of the high-frequency region in Nyquist diagram, and *W* was caused by ion concentration polarization, which was related to the rate of ion conduction in the liquid phase. Imaginary Z'' was mainly expressed through constant phase element (CPE), which directly manifested the inhomogeneity of the membrane interface. With the GCE successively modified, the interfacial impedance was significantly changed. Therefore, by evaluating the mutative trend of *Rct*, the actual surface condition of the GCE could be obtained. As the EIS image shown, the primary GCE exhibited a lower *Rct*. However, with the GOAu-Ru, hybrid DNA probes, MCH and DNA1 gradually modified to the GCE, the *Rct* increased sequentially. When the AgNC modified DNA6 immobilize to DNA3, an evident decrease of the *Rct* was observed. Additionally, ECL signals for each assembly process were also discussed as depicted in Fig. 4C. Apparently, the adsorption of GOAu-Ru presented an intensive ECL signal, which was slightly let down with the immobilizations of non-luminescent substances containing hybrid DNA probes, MCH and DNA1. While the quencher (AgNC modified DNA6) hybridized with the DNA3, the ECL signal was significantly dropped. All the CV, EIS, and ECL response for each modification process jointly verified the biosensor's successful preparation and the ideal biological reaction.

3.6. Assay performance and accuracy valuation of the ECL biosensor

Assay performance of the biosensor for testing various concentrations of NF-κB p50 was investigated, which was illustrated in Fig. 5A. By calculating the degree of the ECL signal increase, the concentrations of the target protein were analyzed. As Fig. 5B given above depicted, the ΔECL intensity increased rapidly with the concentration increase of the NF-κB p50 ranged from 0 pM to 1 nM. Besides, the relationship between ΔECL intensity and concentration of target protein was also investigated (inset in Fig. 5B), the linear equation was $Y = 1.64 + 3.22X$ with $R^2 = 0.998$, in which the Y represented the value difference of ECL between sample at a specific concentration and the blank sample ranged from 0 to 300 pM, X represented the concentrations of target proteins. What is more, the limit of the detection (LOD) was 9.1 pM, which was comparable to previous work shown in Table S3 in the past few years. We also investigated the assay performance in diluted nuclear extracts to evaluate the validity of the sensor. Table 1 showed that the recoveries in Tris-HCl buffers with and without 10-fold diluted nuclear extracts ranged from 99.1–104.6% and 95.8–104.3%, respectively, indicating that the strategy with excellent validity was applicable in clinical detections. In order to evaluate the accuracy of the strategy for NF-κB p50 detection, the sample was assessed by a commercially available NF-κB p50 ELISA kit. Our strategy's experimental results were compared with those of the ELISA kit, which were listed in Table S2. The excellent agreement between these methods indicated our analytical approach possessed potentially commercial applications in NF-κB p50 detection and can be considered a viable way for bioanalysis of disease markers.

3.7. Selectivity and reproducibility of the ECL biosensor

The specificity of the ECL system was verified by four selected non-specific proteins, the concentration of which was 10-folded that of the target protein (100 pM), consisting of bovine serum albumin (BSA), acid-binding immunoglobulin (Ig)-like lectin 5 (Siglec-5), carcinoembryonic antigen (CEA), and interferon-γ (IFN-γ). As depicted in Fig. 5C,

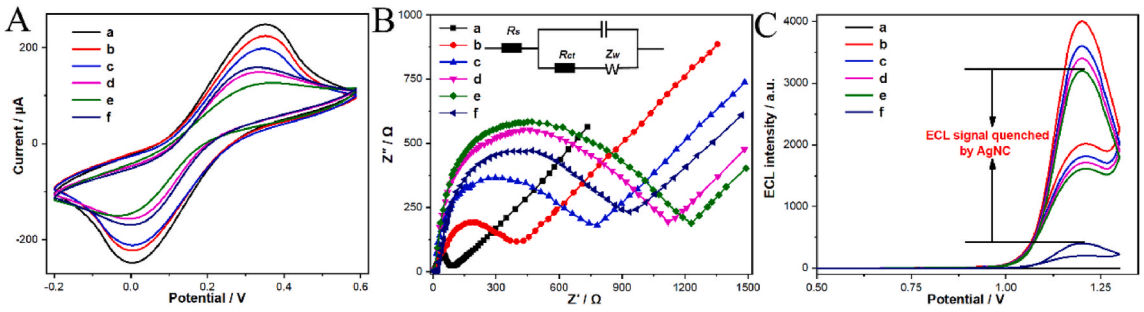

Fig. 4. (A) CV curve, (B) Nyquist plot of impedance spectra and (C) ECL responses for (a) bare GCE, (b) GOAu-Ru/GCE, (c) hybrid DNA probes/GOAu-Ru/GCE, (d) MCH/hybrid DNA probes/GOAu-Ru/GCE, (e) DNA1/MCH/hybrid DNA probes/GOAu-Ru/GCE, (f) AgNC/DNA1/MCH/hybrid DNA probes/GOAu-Ru/GCE.

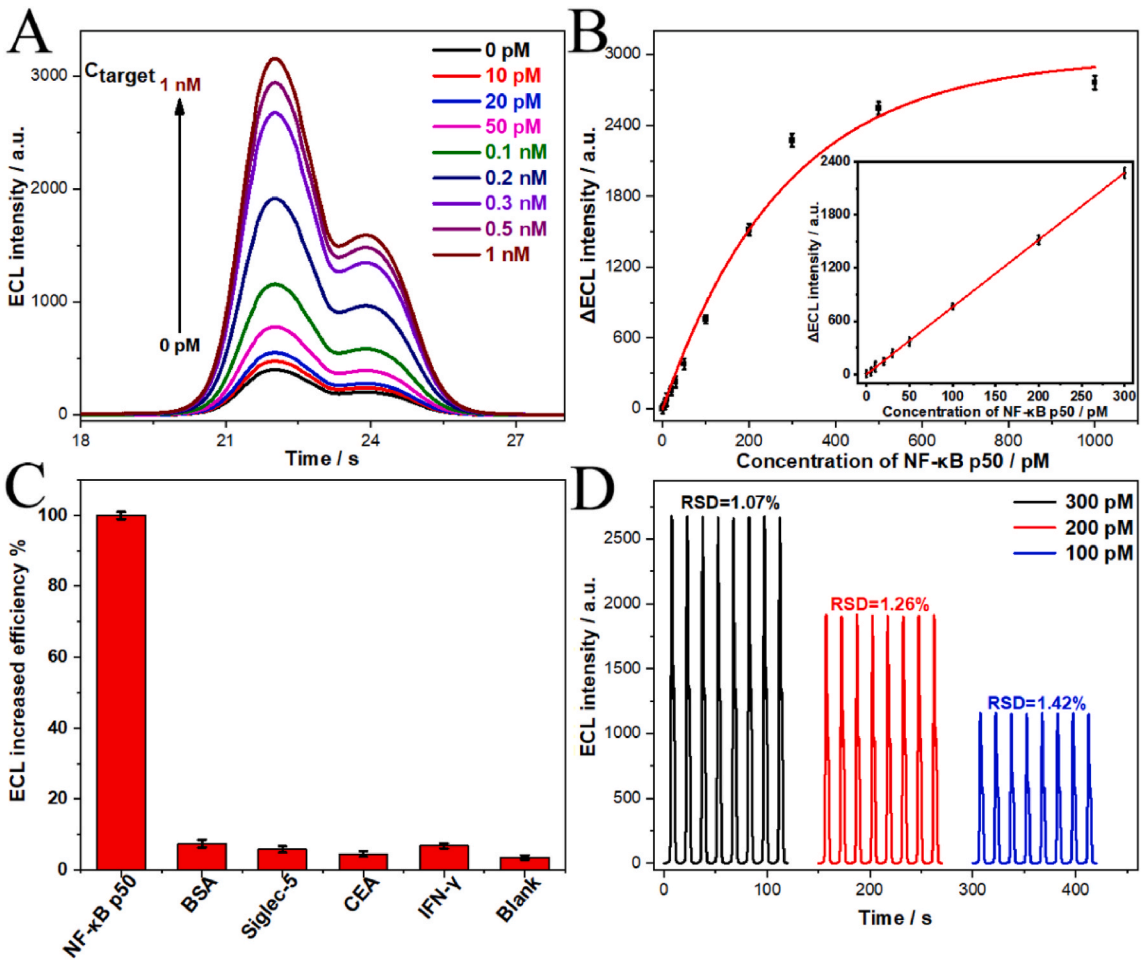

Fig. 5. (A) ECL responses at different concentrations of NF-κB p50. (B) The plot of ECL signal versus concentration of target protein ranged from 0 pM to 1 nM. The inset was the calibration curve in the range of 0–300 pM. (C) Specificity of the strategy on non-specific proteins. The concentrations of non-specific proteins were 10-fold that of the target protein (100 pM). (D) Reproducibility of the biosensor under 8 continuous potential scannings from −1−1.3 V.

Table 1
Recovery tests of the ECL biosensor in detecting NF-κB p50 incubated by Tris-HCl buffer (1) and Tris-HCl buffer containing10-fold diluted nuclear extracts (2).

		NF-κB p50			
Sample	Spiked (pM)	Detected 1 (pM)	Recovery 1 (%)	Detected 2 (pM)	Recovery 2 (%)
1	0	0	N/A	60.27	N/A
2	10	10.23	102.3	70.19	99.2
3	20	19.16	95.8	81.18	104.6
4	50	52.16	104.3	112.46	104.4
5	100	99.51	99.5	163.31	103.0
6	200	204.57	102.3	258.52	99.1

the quenching efficiency was much lower when BSA, Siglec-5, CEA, IFN-γ existed, which was a similar quenching effect with the blank sample. In contrast, a much higher quenching efficiency was noticed in the presence of NF-κB p50, revealing the well-designed biosensor was with excellent selectivity towards NF-κB p50. In addition, the stability of the ECL signal was explored by estimating consequent potential canning of 8 cycles. The Fig. 5D showed the ECL response under different concentrations of target protein, the corresponding relative standard deviations (RSD) calculated were within the acceptable range (5%), denoting the sensing method was with excellent reproducibility and highly appliable value.

3.8. Inhibition assays

NF-κB plays an essential role in a variety of diseases. The constitutive activity of NF-κB has been grabbled in many cancers, and it becomes more and more critical amid the new coronavirus cytokine storm. Therefore, the development of strategies to block the expression of NF-κB activity can be the primary goal of drug development for tumour therapy or new coronavirus therapy. The activity of NF-κB can be inhibited by impeding any step of its signal pathway. However, the most straightforward and effective solution is to prevent the binding of NF-κB to DNA. Moreover, the research method for an inhibitor can be transformed into a screening platform for a class of drugs. Therefore, we use our designed biosensors to study inhibitors of NF-κB p50. We chose (−)-DHMEQ as an inhibitor research model, which covalently binds to cysteine through DNA to inhibit NF-κB activity. In our modified experiments, the fixed concentration of NF-κB p50 was chosen to be 200 pM (50 μL), and the corresponding electrochemical signals of the biosensor was obtained from detecting the mixture of NF-κB p50 solution and various concentrations of (−)-DHMEQ (50 μL). It can be seen from Fig. 6 that as the concentration of inhibitor increases, the ECL signal decreased. By fitting the data and calculating the half-maximum inhibitory concentration of (−)-DHMEQ, the half-maximum inhibitory concentration value abbreviated as (IC_{50}) was 0.83 nM. Therefore, our method can be used to screen drugs related to NF-κB p50 inhibitors and calculate IC_{50} values.

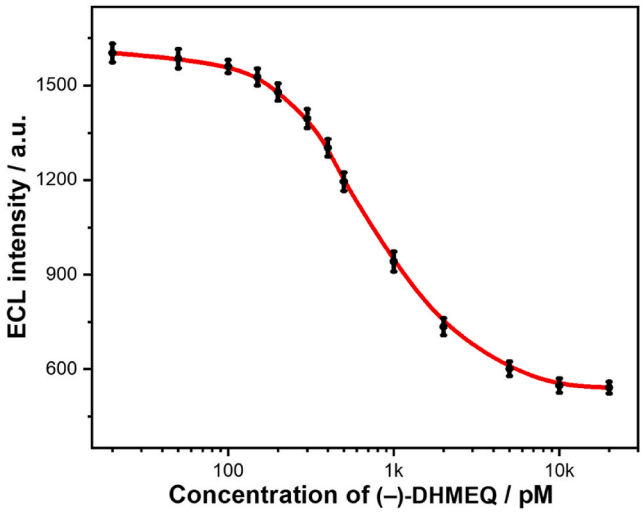

Fig. 6. Relationship between the ECL peak intensity and the logarithms of the concentration of (−)-DHMEQ for illustrating the inhibition effect of this strategy. Five duplicate measurements got every datum and the presented data were the results of the average values of the parallel experiments. The fixed concentration of NF-κB p50 was 200 pM (50 μL) and the calculated IC_{50} was 0.83 nM in this inhibitor assay.

4. Conclusions

In short, we emoloy GOAu-Ru as the electrochemiluminescence signal-generating material and use the entropy-driven auxiliary signal amplification to achieve ultra-sensitive detection of NF-κB p50. The ECL sensor has successfully simplified the detecting methods, obtaining multiple sets of experimental data with down to picomole concentration (LOD) within hours. No expensive antibodies are involved in the experiments, therefore significantly reducing the costs of the assays. Besides, the sensor exhibits extremely high specificity and signal stability during the assays. The sensor can also screen NF-κB p50 inhibitors and measure inhibitor IC_{50}. Therefore, this method not only expands the application range of GOAu-Ru materials and AgNC, but also provides up-and-coming analytical techniques for biomedical research related to TFs. More importantly, the study offers a reliable idea for the development of a new coronavirus cytokine storm and related drugs.

CRediT authorship contribution statement

Kai Zhang: Conceptualization, Writing - review & editing. **Zhenqiang Fan:** Data curation, Characterization, Writing - review & editing. **Bo Yao:** Software. **Tingting Zhang:** Testing. **Yuedi Ding:** Validation. **Sha Zhu:** Testing. **Minhao Xie:** Writing - review & editing.

Declaration of competing interest

The authors declare that they have no known competing financial interests or personal relationships that could have appeared to influence the work reported in this paper.

Acknowledgment

This work was supported by the National Natural Science Foundation of China (21705061), the Jiangsu Provincial Key Medical Discipline (Laboratory) (ZDXKA2016017), and the Innovation Capacity Development Plan of Jiangsu Province (BM2018023).

Appendix A. Supplementary data

Supplementary data to this article can be found online at https://doi.org/10.1016/j.bios.2020.112942.

References

Bath, J., Green, S.J., Turberfield, A.J., 2005. A free-running DNA motor powered by a nicking enzyme. Angew. Chem. Int. Ed. 44 (28), 4358–4361.
Brutzer, H., Schwarz, F.W., Seidel, R., 2012. Scanning evanescent fields using a pointlike light source and a nanomechanical DNA gear. Nano Lett. 12 (1), 473–478.
Cao, A., Zhang, C.-y., 2013. Real-time detection of transcription factors using target-converted helicase-dependent amplification assay with zero-background signal. Anal. Chem. 85 (4), 2543–2547.
Chen, A., Zhao, M., Zhuo, Y., Chai, Y., Yuan, R., 2017. Hollow porous polymeric nanospheres of a self-enhanced ruthenium complex with improved electrochemiluminescent efficiency for ultrasensitive aptasensor construction. Anal. Chem. 89 (17), 9232–9238.
Chen, G.-H., Chen, W.-Y., Yen, Y.-C., Wang, C.-W., Chang, H.-T., Chen, C.-F., 2014. Detection of mercury (ii) ions using colorimetric gold nanoparticles on paper-based analytical devices. Anal. Chem. 86 (14), 6843–6849.
Chen, J., Luo, Z., Sun, C., Huang, Z., Zhou, C., Yin, S., Duan, Y., Li, Y., 2019. Research progress of DNA walker and its recent applications in biosensor. TrAC Trends Anal. Chem. (Reference Ed.) 120, 115626.
Collinson, M.M., Taussig, J., Martin, S.A., 1999. Solid-state electrogenerated chemiluminescence from gel-entrapped ruthenium(ii) tris(bipyridine) and tripropylamine. Chem. Mater. 11 (9), 2594–2599.
Fan, Z., Wang, J., Hao, N., Li, Y., Yin, Y., Wang, Z., Ding, Y., Zhao, J., Zhang, K., Huang, W., 2019. Ultrasensitive detection of transcription factors with a highly-efficient diaminoterephthalate fluorophore via an electrogenerated chemiluminescence strategy. Chem. Commun. 55 (79), 11892–11895.
Gao, Y., Zhou, Y., Chandrawati, R., 2020. Metal and metal oxide nanoparticles to enhance the performance of enzyme-linked immunosorbent assay (elisa). ACS Appl. Nano Mater. 3 (1), 1–21.
Ge, J., Zhao, Y., Li, C., Jie, G., 2019. Versatile electrochemiluminescence and electrochemical "on–off" assays of methyltransferases and aflatoxin b1 based on a novel multifunctional DNA nanotube. Anal. Chem. 91 (5), 3546–3554.
Guan, W.-J., Ni, Z.-Y., Hu, Y., Liang, W.-H., Ou, C.-Q., He, J.-X., Liu, L., Shan, H., Lei, C.-L., Hui, D.S.C., Du, B., Li, L.-J., Zeng, G., Yuen, K.-Y., Chen, R.-C., Tang, C.-L., Wang, T., Chen, P.-Y., Xiang, J., Li, S.-Y., Wang, J.-L., Liang, Z.-J., Peng, Y.-X., Wei, L., Liu, Y., Hu, Y.-H., Peng, P., Wang, J.-M., Liu, J.-Y., Chen, Z., Li, G., Zheng, Z.-J., Qiu, S.-Q., Luo, J., Ye, C.-J., Zhu, S.-Y., Zhong, N.-S., China Medical Treatment Expert Group for, C., 2020. Clinical characteristics of coronavirus disease 2019 in China. N. Engl. J. Med. 382, 1708–1720.
Hlavac, N., VandeVord, P.J., 2019. Astrocyte mechano-activation by high-rate overpressure involves alterations in structural and junctional proteins. Front. Neurol. 10, 99.
Holzhauser, T., Stephan, O., Vieths, S., 2002. Detection of potentially allergenic hazelnut (corylus avellana) residues in food: A comparative study with DNA pcr-elisa and protein sandwich-elisa. J. Agric. Food Chem. 50 (21), 5808–5815.
Huang, C., Wang, Y., Li, X., 2020. Clinical features of patients infected with 2019 novel coronavirus in wuhan, China (vol 395, pg 497, 2020). Lancet 395 (10223), 496-496.
Huang, J., Zhu, L., Ju, H., Lei, J., 2019. Telomerase triggered DNA walker with a superhairpin structure for human telomerase activity sensing. Anal. Chem. 91 (11), 6981–6985.
Jiang, D., Jia, Y., Zhou, Y., Jarrett, H.W., 2009. Two-dimensional southwestern blotting and characterization of transcription factors on-blot. J. Proteome Res. 8 (7), 3693–3701.
Jiang, M.-H., Li, S.-K., Zhong, X., Liang, W.-B., Chai, Y.-Q., Zhuo, Y., Yuan, R., 2019. Electrochemiluminescence enhanced by restriction of intramolecular motions (rim): tetraphenylethylene microcrystals as a novel emitter for mucin 1 detection. Anal. Chem. 91 (5), 3710–3716.
Li, X.-M., Li, W., Ge, A.-Q., Chen, H.-Y., 2010. Logic-based dual-functional DNA tweezers with protein and small molecule as mechanical activators. J. Phys. Chem. C 114 (50), 21948–21952.
Lin, Y., Jia, J., Yang, R., Chen, D., Wang, J., Luo, F., Guo, L., Qiu, B., Lin, Z., 2019. Ratiometric immunosensor for gp73 detection based on the ratios of electrochemiluminescence and electrochemical signal using DNA tetrahedral nanostructure as the carrier of stable reference signal. Anal. Chem. 91 (5), 3717–3724.
Mahmudpour, M., Roozbeh, J., Keshavarz, M., Farrokhi, S., Nabipour, I., 2020. Covid-19 cytokine storm: the anger of inflammation. Cytokine 133, 155151.
Markopoulos, G.S., Roupakia, E., Marcu, K.B., Kolettas, E., 2019. Epigenetic regulation of inflammatory cytokine-induced epithelial-to-mesenchymal cell transition and cancer stem cell generation. Cells 8 (10), 1143.
Nie, Y., Yuan, X., Zhang, P., Chai, Y.-q., Yuan, R., 2019. Versatile and ultrasensitive electrochemiluminescence biosensor for biomarker detection based on nonenzymatic amplification and aptamer-triggered emitter release. Anal. Chem. 91 (5), 3452–3458.
Parks, M.E., Baird, E.E., Dervan, P.B., 1996. Recognition of 5'-(a,t) gg(a,t)2-3' sequences in the minor groove of DNA by hairpin polyamides. J. Am. Chem. Soc. 118 (26), 6153–6159.
Potoyan, D.A., Zheng, W., Ferreiro, D.U., Wolynes, P.G., Komives, E.A., 2016. Pest control of molecular stripping of nfκb from DNA transcription sites. J. Phys. Chem. B 120 (33), 8532–8538.
Rothemund, P.W.K., 2006. Folding DNA to create nanoscale shapes and patterns. Nature 440 (7082), 297–302.
Seeman, N.C., 1982. Nucleic acid junctions and lattices. J. Theor. Biol. 99 (2), 237–247.

Shao, W., Wei, H.-J., Qiao, J.-Y., Zhao, Y.-C., Sun, Y.-M., Zhou, Y.-X., Cheng, J., 2005. Parallel profiling of active transcription factors using an oligonucleotide array-based transcription factor assay (oatfa). J. Proteome Res. 4 (4), 1451–1456.
Terpos, E., Ntanasis-Stathopoulos, I., Elalamy, I., Kastritis, E., Sergentanis, T.N., Politou, M., Psaltopoulou, T., Gerotziafas, G., Dimopoulos, M.A., 2020. Hematological findings and complications of covid-19. Am. J. Hematol. 95 (7), 834–847.
Xu, Z., Chang, Y., Chai, Y., Wang, H., Yuan, R., 2019. Ultrasensitive electrochemiluminescence biosensor for speedy detection of microrna based on a DNA rolling machine and target recycling. Anal. Chem. 91 (7), 4883–4888.
Yang, X., Yu, Y.-Q., Peng, L.-Z., Lei, Y.-M., Chai, Y.-Q., Yuan, R., Zhuo, Y., 2018. Strong electrochemiluminescence from mof accelerator enriched quantum dots for enhanced sensing of trace ctni. Anal. Chem. 90 (6), 3995–4002.
Ye, J., Zhu, L., Yan, M., Zhu, Q., Lu, Q., Huang, J., Cui, H., Yang, X., 2019. Dual-wavelength ratiometric electrochemiluminescence immunosensor for cardiac troponin i detection. Anal. Chem. 91 (2), 1524–1531.
Yin, J., Gan, P., Zhou, F., Wang, J., 2014. Sensitive detection of transcription factors using near-infrared fluorescent solid-phase rolling circle amplification. Anal. Chem. 86 (5), 2572–2579.
Zhang, B., Zhang, F., Zhang, P., Shen, D., Gao, X., Zou, G., 2019a. Ultrasensitive electrochemiluminescent sensor for microrna with multinary zn–ag–in–s/zns nanocrystals as tags. Anal. Chem. 91 (5), 3754–3758.
Zhang, D.Y., Turberfield, A.J., Yurke, B., Winfree, E., 2007. Engineering entropy-driven reactions and networks catalyzed by DNA. Science 318 (5853), 1121–1125.
Zhang, K., Fan, Z., Li, H., Zhao, J., Xie, M., 2020. Determination of the concentration of transcription factor by using exonuclease iii-aided amplification and gold nanoparticle mediated fluorescence intensity: a new method for gene transcription related enzyme detection. Anal. Chim. Acta 1104, 132–139.
Zhang, K., Huang, W., Li, H., Xie, M., Wang, J., 2019b. Ultrasensitive detection of herg potassium channel in single-cell with photocleavable and entropy-driven reactions by using an electrochemical biosensor. Biosens. Bioelectron. 132, 310–318.
Zhang, Y., Hu, J., Zhang, C.Y., 2012. Sensitive detection of transcription factors by isothermal exponential amplification-based colorimetric assay. Anal. Chem. 84 (21), 9544–9549.
Zhang, Y., Wang, L., Luo, F., Qiu, B., Guo, L., Weng, Z., Lin, Z., Chen, G., 2017. An electrochemiluminescence biosensor for kras mutations based on locked nucleic acid functionalized DNA walkers and hyperbranched rolling circle amplification. Chem. Commun. 53 (20), 2910–2913.
Zhou, M., Liang, X., Mochizuki, T., Asanuma, H., 2010. A light-driven DNA nanomachine for the efficient photoswitching of rna digestion. Angew. Chem. Int. Ed. 49 (12), 2167–2170.